WIND
ENERGY
SCIENCE

Comparison between upwind and downwind designs of a 10 MW wind turbine rotor

Pietro Bortolotti, Abhinav Kapila, and Carlo L. Bottasso

Wind Energy Institute, Technische Universität München, 85748 Garching, Germany

Correspondence: Carlo L. Bottasso (carlo.bottasso@tum.de)

Abstract. The size of wind turbines has been steadily growing in the pursuit of a lower cost of energy by an increased wind capture. Within this trend, the vast majority of wind turbine rotors have been designed based on the conventional three-bladed upwind concept. This paper aims at assessing the optimality of this configuration with respect to a three-bladed downwind design, with and without an actively controlled variable coning used to reduce the cantilever loading of the blades. Results indicate that a conventional design appears difficult to beat even at these turbine sizes, although a downwind nonaligned configuration might be an interesting alternative.

1 Introduction

The size of wind turbines in terms of both rotor diameter and nameplate power has been dramatically increasing over the last few decades. The key driver behind this spectacular growth has been the reduction in levelized cost of energy (CoE), which typically benefits from an increase in energy capture. The trend is expected to continue as more countries promote new offshore installations and onshore wind increases its presence in regions of low average wind speeds. In addition, in countries characterized by a high penetration of wind power such as Denmark and Germany, the structure of the electricity market tends to favor larger rotor sizes. In fact, the price of electricity in these markets is increasingly correlated with the availability of wind power. At times when wind power is abundant, electric grids may experience an excess of power generation, which in turn leads spot market prices to markedly drop (Badyda and Dylik, 2017), ultimately reducing the importance of power production in high winds.

The growth in rotor diameters is, however, pushing the limits of conventional wind turbine configurations. For example, one especially important design driver of very long blades is the minimum clearance between tip and tower to prevent strikes. In fact, the design of large upwind rotors is often driven by tip-clearance requirements (Bortolotti et al., 2016, 2018). To meet this constraint, designers are increasingly adopting a combination of thick airfoils and high-

modulus composites to increase the out-of-plane stiffness of the blades. Together with an increase in blade prebend, rotor cone and nacelle uptilt angles, these design choices help satisfy the tower clearance constraint. Nonetheless, achieving CoE reductions by upscaling conventional upwind configurations is an increasingly challenging task.

In this scenario, the recent literature suggests that downwind rotor configurations may offer the opportunity to generate lower CoE values compared to traditional upwind ones (Frau et al., 2015; Ning and Petch, 2016). Cost reductions could be obtained in downwind configurations thanks to lighter and more flexible blades, made possible by a relaxed tower clearance constraint. In addition, an increased annual energy production (AEP) could be generated by reduced cone and uptilt angles, as well as by a favorable blockage effect generated by the nacelle. In fact, the presence of the nacelle located upwind of the rotor has the effect of redirecting the flow towards the outboard part of the blade. This way, the flow speeds up towards blade sections characterized by thinner and more efficient airfoils and, as a result, a higher AEP is produced. An experimental campaign on subscale models showed an increase in AEP equal to 5 % against an increase of 3 % of rotor thrust (Kress et al., 2015a). Furthermore, in sites characterized by upflow angles, such as hills and ridges, the uptilt angle improves the alignment of the rotor with the incoming wind in the downwind case, while it

has the opposite effect in the upwind one. Lastly, the weathercock stability of downwind rotors could, at least in principle, be exploited to reduce the cost of the yaw system (Kress et al., 2015a).

Clearly, these benefits would not come for free, and downwind rotors struggle against a major disadvantage, namely an increased tower shadow effect (Reiso, 2013). This results into two main negative effects compared to equivalent upwind designs. First, fatigue loading typically increases due to a higher one-per-revolution harmonic blade excitation (Manwell et al., 2009; Kress et al., 2015b). Secondly, higher noise emissions are generated due to the blade interference with the tower wake, especially in the low frequency range of the noise spectrum (Madsen et al., 2007). These two aspects have been especially important for early onshore machines and, as a result, most modern designs worldwide adopt the upwind configuration. One notable exception to this situation is represented by the downwind machines developed by Hitachi Ltd. and installed in Japan (Kress et al., 2015b).

An additional potential advantage of downwind rotors is the possibility of achieving the so-called "load alignment" along the blades, a novel concept proposed and investigated in Ichter et al. (2016), Loth et al. (2017) and Noyes et al. (2018). Load alignment may be seen as bio-inspired by palm trees, which sustain storms by bending downwind and aligning their leaves in the wind direction. In turn, this has the effect of turning cantilever loads into tensile ones. In Ichter et al. (2016), Loth et al. (2017) and Noyes et al. (2018) this concept is investigated by designing a 13.2 MW two-bladed downwind rotor, which exhibits a decreased CoE in comparison to an equivalent upwind three-bladed configuration. This claim is supported by reduced out-of-plane fatigue and ultimate loads that lead to a reduction of blade mass.

The goal of this work is the comparison of three-bladed upwind rotor configurations with three-bladed downwind designs, including load alignment. The present work does not consider the case of teetering two-bladed rotors. Similarly to Ning and Petch (2016), the present investigation performs a detailed aerostructural optimization to minimize the CoE of each wind turbine configuration. The main difference of this study with respect to the existing literature is that the analyses conducted herein are characterized by a higher fidelity of the simulation models and by a more complete set of load cases, including shutdowns. In fact, these are often found to be driving the design of downwind wind turbine blades and, therefore, should be part of the design process.

The design framework adopted in the present investigation is `Cp-Max`, whose detailed description is reported in Bortolotti et al. (2016, 2018) and references therein. The comprehensive design procedures implemented in `Cp-Max` account for all design constraints typically included in an industrial design context and allow one to consider the various multidisciplinary couplings of the problem, which are necessary to identify CoE-optimal constraint-satisfying solutions. This is achieved by balancing turbine capital cost and AEP. The

design optimization procedures are driven by the combination of two cost models. A first model developed at Sandia National Laboratories (Johans and Griffith, 2013) is used to estimate the blade cost. This model overcomes the use of a simplified relationship between blade mass or blade length versus blade cost, and it accounts for material, equipment and labor costs. CoE is estimated by the cost model developed within the INNWIND.EU project (INNWIND.EU, Deliverable 1.23, 2014). This second cost model is especially focused on next-generation offshore wind turbine designs.

The paper is structured as follows. Section 2 reviews the aeroservoelastic simulation models used in the study, the load-alignment concept and a short summary of the aerostructural design procedures. Then, Sect. 3 discusses the wind turbine configuration used as baseline and the novel downwind designs, which are compared in terms of loads, performance and costs. The study is closed in Sect. 4, where the main conclusions of the study are summarized.

2   Modeling, simulation and design

This work is concerned with the evaluation of design configurations of wind turbines. This activity is supported by the wind turbine design framework `Cp-Max`, which uses aeroservoelastic models implemented within the wind turbine simulator `Cp-Lambda` coupled to a model-based controller, which are described in Sects. 2.1 and 2.2, respectively. This background information is followed by Sect. 2.3, where the load-alignment design concept is reviewed. Finally, Sect. 2.4 briefly recalls the design procedures implemented in `Cp-Max`.

2.1   Aeroelasticity

The aeroelastic behavior of the various wind turbine design configurations is computed in this work with the aeroservoelastic simulator `Cp-Lambda` (Code for Performance, Loads and Aeroelasticity by Multi-Body Dynamic Analysis). `Cp-Lambda` implements a multibody formulation for flexible systems with general topologies and features a library of elements, which includes rigid bodies, nonlinear flexible elements, joints, actuators and aerodynamic models (Bottasso et al., 2006; Bauchau, 2011). Sensor and control elements enable the implementation of generic control laws. The multibody index-3 formulation is expressed in terms of Cartesian coordinates, while constraints are enforced by scaled Lagrange multipliers. In this study, the rotor blades and the tower are modeled by nonlinear geometrically exact shear and torsion-deformable beam models. Fully populated stiffness matrices account for couplings generated by anisotropic composite materials. Flexible components are discretized in space, leading to a system of differential algebraic equations in the time domain.

The blade aerodynamic characteristics are defined by lifting lines, which include the spanwise chord and twist distri-

butions as well as sectional aerodynamic coefficients, given in tabular form and parameterized in terms of Reynolds number. The calculation of aerodynamic loads is performed at selected points, called air stations, along each lifting line. Each air station is rigidly connected to an associated beam cross section, and moves with it. As a consequence, the local airflow kinematics at each air station include the contributions due to blade movement and deformation. In addition, the effects of the wake are modeled by a classical blade element momentum (BEM) model based on annular stream tube theory with wake swirl and unsteady corrections (Hansen, 2008), or by the dynamic inflow model of Pitt and Peters (1981) and Peters and He (1995). The aerodynamic description is completed by root and blade tip losses, unsteady aerodynamic corrections, dynamic stall, 3-D blade root delayed stall, and upwind and downwind rotor–tower interference models. For upwind rotors, the tower shadow effect is modeled by assuming an incompressible laminar flow around a cylinder, while the model of Powles (1983) is used in the downwind case. No dedicated nacelle blockage model is included in the simulation of downwind configurations, which might lead to a slight underestimation of power capture.

A parameterized model of the blade structure is defined by choosing a number of control stations. At each section of interest, airfoils, blade topology, composite mechanical properties and the geometry of the structural members are given, and the cross-sectional solver ANBA (Giavotto et al., 1983) is used to produce the associated six-by-six stiffness matrix and sectional blade properties. In turn, these properties are used to define the corresponding beams in the Cp-Lambda model.

2.2 Model-based controller

The virtual wind turbines developed in this study are governed over their entire operating range by a controller interfaced with Cp-Lambda through external dynamic libraries. A supervisory unit manages the machine behavior by switching among different operating states and handling emergencies. Pitch and torque are handled by suitable controllers operating in a closed loop with the machine on the basis of data supplied by sensor models. All wind turbine models developed in the current study use the linear quadratic regulator (LQR) described in Bottasso et al. (2012). This model-based formulation allows for a straightforward update of the control laws during design, as its underlying reduced-order model can be readily updated whenever the wind turbine parameters change, thereby automatically producing new sets of gains that work in combination with the new design. While probably not superior to other classical pitch and torque controllers used in industrial practice, this method is found to be useful in this research context as it allows for an automatic tuning of the control laws throughout the design process.

The LQR controller is synthesized by means of simulations run in steady wind conditions to evaluate the aerodynamic performance of the machine for a three-dimensional grid of tip-speed ratios λ, blade pitch angles β and wind speeds V. These simulations take into account the aeroelastic effects of the flexible bodies of the entire wind turbine model and include the computation of aerodynamic, inertial and gravitational loads. The aerodynamic performance is evaluated by extracting internal forces at the hub, which yield the thrust force and shaft torque. By nondimensionalizing these values, one obtains the thrust C_T and power C_P coefficients, as functions of λ, β and V, which are stored in look-up tables. Based on the C_P tables, the regulation trajectory of the machine is computed, defining the control parameters (pitch, rotational speed and torque) for regions II and III, defined as the operating regions between cut-in wind speed V_{in} and rated wind speed V_r, and between V_r and cut-out wind speed V_{out}, respectively (Bottasso et al., 2012). In region II, C_P is maximized, while in region III power is held constant. In addition, the rotor is regulated to comply with a possible limit on the maximum blade tip speed, which may result in the appearance of a transition region II$\frac{1}{2}$ between the partial and full loading regimes.

2.3 Load-aligned rotor

The concept of load alignment for wind turbine rotors has been introduced and developed in Ichter et al. (2016), Loth et al. (2017) and Noyes et al. (2018). The idea consists of designing a suitably prebent blade in order to align the resultant of the various forces acting on the blade with its axis. The goal of such alignment is to convert out-of-plane cantilever forces into tensile ones, which can be resisted by a lighter-weight structure.

The primary forces acting on a wind turbine rotor are the thrust force F_t, centrifugal force F_c and gravitational force F_g. Since F_t greatly depends on the wind speed and F_c on the rotational speed, which in turn depends on the wind speed as well, the force resultant changes magnitude and direction over time. An exact load alignment can then be achieved only by a truly morphing blade that adjusts its out-of-plane shape based on wind speed. In this study, the prebent shape of the blade is instead assumed to be frozen, while an out-of-plane load alignment at blade root is sought by means of three flap hinges and three corresponding actuators. The goal of the hinges and actuators is to actively control the cone angle γ of each blade. Figure 1 shows a schematic view of this concept.

The resultant of the three forces F_t, F_c and F_g does not only depend on wind speed, but also changes its direction with the azimuthal position of the blade. This change is caused by the periodic variation in the gravitational loading F_g acting on the rotating blade, and by the atmospheric wind shear influencing F_t. As a result, an exact load alignment at blade root can only be achieved by an individual control of the angle γ for each one of the blades. This would, how-
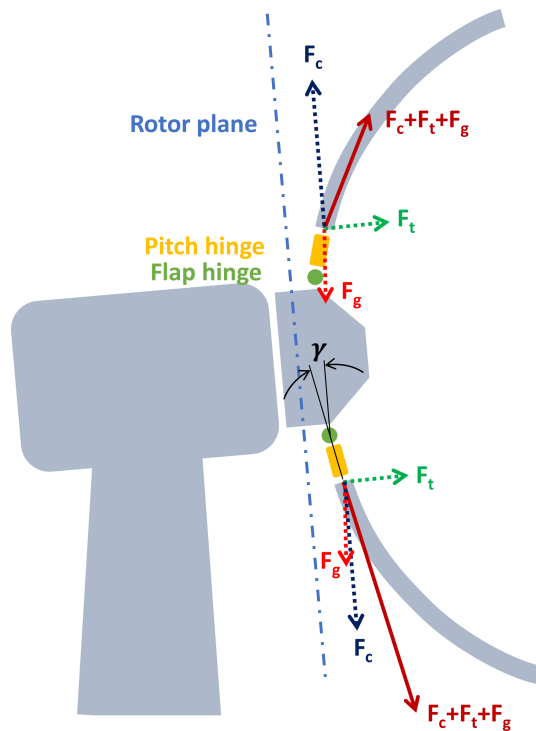
Figure 1. Schematic view of the active load-alignment concept.

ever, require a flap actuator control rate of several degrees per second. In addition, individual flapping of the blades would break the axial symmetry of the rotor, generating major rotor mass imbalances. Because of these reasons, an average (collective) γ is used for the three blades, which is changed based on wind speed. A maximum value is set for the blade root out-of-plane moments across one whole rotor revolution. When this threshold value is exceeded, the rotor blades are collectively coned by an angle γ. The coning value is chosen based on a 30 s moving average of the wind speed, which removes fast fluctuations and aims at identifying the current mean operating condition. To avoid inaccuracies of the nacelle anemometer, a rotor-equivalent wind speed may be obtained by a suitable estimator (Soltani et al., 2013).

2.4 Blade aerostructural design optimization

`Cp-Max` implements wind turbine design methods that integrate a blade aerodynamic optimization with a blade and tower structural optimization, within an overall turbine optimization procedure. The optimization loops are structured following a nested architecture and the overall design goal is the minimization of the CoE. In this study, only the aerodynamic and the structural optimization loops of the blade are used, while the tower is held frozen. For a more complete overview of the design methodologies implemented in `Cp-Max`, interested readers can refer to Bortolotti et al. (2016) and references therein.

The aerodynamic optimization loop is used here to compute an optimal twist distribution for all designed blades. However, the planform shape of all blades was kept the same as the baseline design. Twist is parameterized along the blade span at a number of stations. In each station, an optimization variable is defined, corresponding to an additive gain added to the local twist. The actual twist distribution is reconstructed by means of piecewise cubic Hermite interpolating polynomial (PCHIP) splines. The figure of merit of the aerodynamic optimization is the maximization of AEP, while linear and nonlinear constraints are appended to the problem to specify all necessary design requirements and desired features.

The structural optimization aims at the sizing of the blade inner structure for a given outer blade shape. The optimization consists of an iterative loop, beginning with the calculation of the regulation trajectory and the synthesis of the LQR controller gains, which are updated based on the current wind turbine design (Bottasso et al., 2012). Next, a load computation step is performed where a list of design load cases (DLCs) is run. The postprocessed results of these analyses are used to compute the load envelopes at a number of verification stations along the three blades. The rainflow counting required to estimate fatigue damage is also performed here. Given these inputs, the actual structural sizing is computed by means of a sequential quadratic programming (SQP) algorithm, which is well suited to problems with several constraints that are potentially simultaneously active at convergence. The figure of merit of the structural sizing step is blade cost, which is calculated from the Sandia blade cost model (Johans and Griffith, 2013). Gradients are computed by means of forward finite differences. Once the solver converges to a new blade structure, the process iterates back to the tuning of the LQR controller and all steps are repeated until blade cost converges to a predefined tolerance, which is usually set at 1 %.

3 Comparison of design configurations

In this section, the baseline upwind model used as benchmark is first presented in Sect. 3.1. Then, Sect. 3.2 reviews the downwind design configurations developed from the baseline. These are finally compared in Sect. 3.3 in terms of loads, blade mass, blade cost, AEP and CoE. Finally, some critical aspects of the load-aligned solution are discussed in Sect. 3.4.

3.1 Baseline model

The DTU 10 MW reference wind turbine (RWT) platform is here chosen as a significant test case. This wind turbine is a conceptual machine developed by the Wind Energy Department of Denmark Technical University (DTU), freely available in the public domain for research purposes. The main characteristics of the wind turbine are reported in Table 1, while a more complete description of the model and the cri-
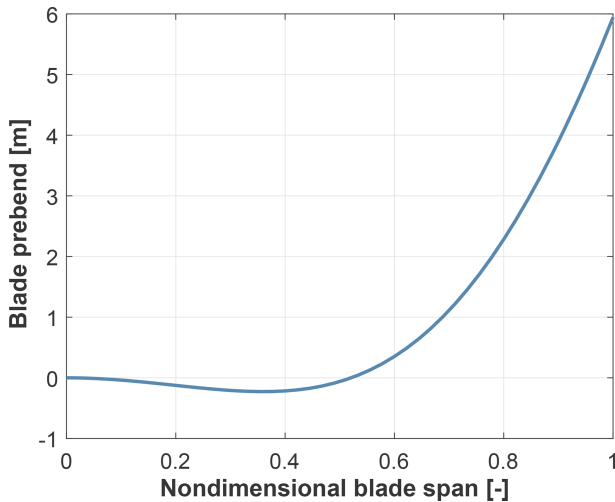
Figure 2. Prebend distribution obtained by `Cp-Max` during the redesign of the 10 MW DTU RWT.

Table 1. Main parameters of the DTU 10 MW RWT.

Data	Value
Wind class	IEC 1A
Rated electrical power	10 MW
Cut-in wind speed V_{in}	$4\,\mathrm{m\,s^{-1}}$
Cut-out wind speed V_{out}	$25\,\mathrm{m\,s^{-1}}$
Rotor diameter	178.3 m
Hub height	119.0 m

a. UW5: upwind redesign with a 5 % larger rotor diameter;

b. DW: downwind design;

c. DW5: downwind redesign with a 5 % larger rotor diameter;

d. DW5LA: downwind redesign with active load alignment and a 5 % larger rotor diameter.

From a multibody modeling point of view, configurations UW, UW5, DW and DW5 have exactly the same topological structure, where the only differences lie in the orientation of the rotor and the presence of actuated flap hinges for the active coning solution of DW5LA, as discussed in Sect. 2.3. The aeroelastic models also differ in the tower shadow effect (downwind or upwind) and in the length of the blades. The hub is identical among the five configurations, while the blade external shapes in UW5, DW5 and DW5LA are geometrically scaled from UW, resulting in rotors with the same solidity and hence also the same tip-speed ratio for maximum power coefficient. The use of a fixed increase in diameter (5 %) for all rotors is meant to highlight the trend of the solution for a given assigned change. An alternative approach might have been to optimize the rotor diameter in order to increase power capture while not exceeding the loads of the baseline design, as done for example in Bortolotti et al. (2016, 2018).

Regarding DW5LA, it was observed that out-of-plane blade root moments cannot be reduced to zero, as this would require a flap angle γ in excess of 45° at rated wind speed. This would lead to a dramatic reduction of the rotor-swept area and, consequently, of the generated AEP. After several tests, it was decided to limit the out-of-plane moment at blade root to 50 % of the maximum steady-state value measured in the UW design, namely 22 MNm. The resulting scheduled values of γ are reported in Fig. 3a, where the angle magnitude is visibly influenced by F_t. Between V_{in} and V_r, the prescribed γ is first held at 0°, since the out-of-plane moment at blade root is below the threshold of 22 MNm. Above a wind speed of $9\,\mathrm{m\,s^{-1}}$, the prescribed γ rapidly increases until rated conditions following the increase in F_t, but keeping the out-of-plane moment at blade root below 22 MNm. Above V_r, blades are pitched into the wind, which results in a reduction of F_t and, consequently, also of γ.

teria used for its design are given in Bak et al. (2013). In this study, the blade prebend distribution is optimized with `Cp-Max` following Sartori et al. (2016), which resulted in the solution reported in Fig. 2. Given this prebend, the blade twist and internal structure are updated by the aerostructural design optimization described in Sect. 2.4, while keeping the planform shape unchanged. For simplicity, a reduced set of DLCs is used, namely DLCs 1.1, 2.3 and 6.2. These represent normal operating conditions, the occurrence of extreme gusts combined with electric faults and the occurrence of a 50-year storm at 12 different values of yaw angle (IEC, 2005). To reduce the computational cost, a single seed per wind speed is used in the turbulent cases, namely DLC 1.1 and DLC 6.2. Although this means that the estimation of fatigue loading and AEP might not be fully converged, it still allows for meaningful comparisons, as the same wind time history for each wind speed was used for all designs.

The blade inner configuration is a fairly standard spar box construction, except for the presence of a third shear web running along part of the blade span close to the trailing edge. Unidirectional fiberglass reinforcements are located at the leading edge (LE) and trailing edge (TE), while an additional reinforcement is superimposed onto the external shell in the blade root region. Table 2 reports the spanwise extension of the structural components and their materials. Transversely isotropic laminae are assumed to have the characteristics summarized in Table 2. The mechanical properties of the resulting composites are computed by classical laminate theory.

3.2 New configurations

The original upwind configuration (UW) is adopted as the starting point to establish a comparison amongst various alternatives.

Table 2. Extent of the structural components and their materials in the blade of the 10 MW wind turbine.

Component	From (% η)	To (% η)	Material type	Longitudinal Young's modulus (MPa)	Transversal Young's modulus (MPa)	Shear modulus (MPa)
Spar caps	1	99.8				
LE–TE reinforcements	10	95	uni-dir. GFRP	41 630	14 930	5047
Root reinforcement	0	45				
First and second shear webs skin	5	99.8	bi-axial GFRP	13 920	13 920	11 500
External shell	0	100	tri-axial GFRP	21 790	14 670	9413
Third shear web skin	22	95				
Shell and webs core	5	99.8	balsa	50	50	150

Tests were also conducted to determine a suitable choice for the coning rate $\dot{\gamma}$. Different values of this parameter from 0.001 to 5° s^{-1} were tested in DLC 1.1, analyzing the resulting out-of-plane blade root moment, as reported in Fig. 3b. Although lower values of $\dot{\gamma}$ could probably be sufficient, a minimum of the loads is identified at 0.25° s^{-1}, which is the value used for the DW5LA design.
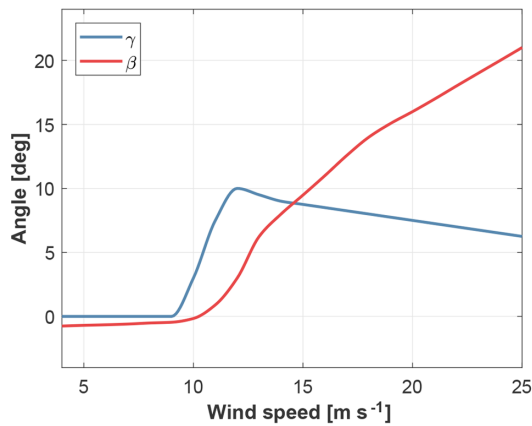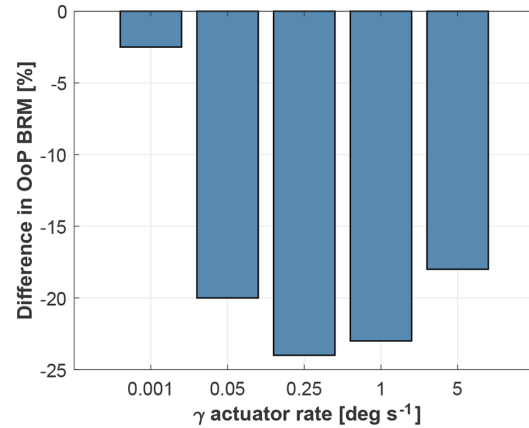
All five configurations were then subjected to an aerodynamic optimization of the twist and a blade structural optimization, as described in Sect. 2.4. Once the two loops converge, the AEP and the CoE are evaluated. The comparison in terms of cost and performance is discussed next.

3.3 Cost and performance comparison

A comparison among the five configurations is presented with the histogram shown in Fig. 4a. First, as already observed in Bortolotti et al. (2016), the current cost models predict a reduction of CoE when the rotor is enlarged. Within this trend, downwind configurations appear to be able to successfully limit the growth in blade mass and cost. This effect is generated by the relaxed tower clearance constraint, which is instead a critical design driver for the UW and UW5 designs. It is, however, interesting to highlight that, although smaller than in the upwind cases, high blade deflections also occur in DW and DW5 during the emergency shutdowns simulated with DLC 2.3. Possibly, optimized shutdown maneuvers could help in generating further mass and cost reductions, but a dedicated study would be needed to more precisely quantify any saving. Although costs are reduced, DW and DW5 generate smaller values of AEP compared to UW and UW5. These reductions are mostly caused by an increased flexibility of the blades, which bend when loaded, in turn reducing the rotor swept area. For a given rotor cone angle, this effect is more detrimental for downwind rotors compared to an equivalent upwind one, as cone and prebend are against the wind in the latter case. The comparison is

instead different as soon as an upflow is present in the incoming wind, which is the typical case of complex terrain conditions when the turbine is located on a hill or close to a ridge. In the present case, an upflow of 5° changes the trend and increases the AEP of the downwind rotors by 0.7 % with respect to their upwind equivalents. This higher AEP is directly converted into a reduction of CoE for both DW and DW5. Notably, changes in AEP are only modest, especially when considering the variety of uncertainties affecting wind turbine simulations. Nonetheless, it should be remarked that a variation of 0.7 % in AEP is not completely negligible, as the two rotors are characterized by the same diameter, they are both optimized in terms of twist and control gains, and they are both subjected to the same wind of class I (where the contribution of region III to AEP is not marginal). In addition, the trend is consistent between the rotors with the baseline diameter, namely UW and DW, and the rotors with the longer blades, namely UW5 and DW5. Finally, tests conducted in steady-state wind conditions corroborate these results. It may be useful to remind the reader that, as mentioned earlier on, nacelle blockage is not accounted for in the simulation models, and its inclusion might generate slight benefits in AEP for DW and DW5. In this scenario, DW5LA has a lower blade mass and cost compared to UW5 and DW5, but also a slightly lower AEP.

A load assessment is then conducted looking at key ultimate and fatigue loads measured at blade root and at the hub. The comparison is reported in Fig. 4b and c. In terms of flapwise blade root moments (FBRM), downwind configurations DW and DW5 help reduce ultimate loads, while they generate approximately the same fatigue loading. On the other hand, DW5LA reduces both ultimate and fatigue loads compared to UW5 and DW5. For the edgewise blade root moment (EBRM), fatigue loads follow the blade mass trend. In the case of fatigue torsional blade root moments (TBRM), an alarming growth is observed for DW5LA. This is due to the increased out-of-plane deformations induced

(a) Cone γ and pitch β angles vs. wind speed for DW5LA.

(b) Effect of γ rate on maximum out-of-plane moment measured at blade root in DLC 1.1.

Figure 3. Cone and cone rate for the DW5LA design.

by a decreased blade stiffness. At the hub, trends are more scattered, with a decrease in the ultimate thrust (ThH) for DW and DW5LA, but an overall marked increase in ultimate out-of-plane bending moments (OoPMH), especially for DW5LA. Finally, the tower base fore–aft (TBFA) moment of DW, DW5 and DW5LA sees a decrease in its ultimate value, but an increase in fatigue except for DW5LA, which stays approximately constant. Notably, ultimate TBFA values are generated in operational conditions for UW and UW5, shutdown conditions in the case of DW, and finally storm conditions for DW5 and DW5LA.

Overall, DW and DW5 are associated with generally lower loading compared to UW and UW5, except for ultimate OoPMH and fatigue TBFA. Larger TBFA may generate an increase in the mass and cost of a steel tower, which is often fatigue driven (Bortolotti et al., 2018). DW5LA is instead effective at reducing loads aligned with the prevailing wind direction, namely FBRM, ThH and TBFA. Furthermore, it benefits from a decreased blade mass and stiffness that result in lower EBRM. This is, however, obtained at the cost of increased torsional moments on the blades (which would impact the pitch system design), and out-of-plane moments at the hub (which would impact the design of the shaft and of the main bearings). A specific, more detailed, design activity would be necessary to more precisely quantify these effects. In addition, DW5LA is prone to several critical aspects, which are assessed in Sect. 3.4.

3.4 Critical aspects of DW5LA and comparison with the literature

As shown in Fig. 5a, compared to configuration DW5, power losses of the design solution DW5LA are limited to wind speeds around rated conditions. However, active load alignment in turbulent dynamic cases is only partially effective. In fact, although blade root moments do indeed decrease thanks

to active coning, moments at other points along the blade span are not significantly affected. It is speculated that a reduction of moments throughout a larger portion of blade span would necessitate a truly morphing solution, with adjustable prebend. As a result of the only partial effectiveness of active coning, the blade cost of DW5LA is not significantly reduced compared to the one of configuration DW5. In addition, loads generated during storm conditions are not necessarily alleviated by active coning. In fact, folding the rotor will reduce its swept area, but it will also dramatically move the rotor center of gravity away from the tower, resulting in very large loading of the structure and foundations. For example, aeroelastic simulations were performed in storm conditions with a wind misaligned by $\pm 30°$, having folded the blades with a value of $\gamma = 60°$. Although a more sophisticated computational fluid dynamics analysis would be needed to accurately predict aerodynamic forces at such angles of attack, bending moments at the hub were doubled, while tower base moments increased by 40 %.

Finally, for the chosen coning rate $\dot{\gamma}$ the actuators of configuration DW5LA have a nonnegligible power consumption. Figure 5b shows the consumption estimated during DLC 1.1 for the case without a power recovery system (label woRec) and with a recovery system having an efficiency of 80 % (label wRec). Such solution, although technologically complex, would be able to recover most of the energy used by the actuators.

Overall, given the fact that the joints and actuators necessary for active coning would certainly pose serious engineering challenges and associated costs, a conventional downwind configuration would appear here to be more interesting than an actively load-aligned one.

These conclusions, which are in line with the results found in Ning and Petch (2016), are somewhat less promising than the ones presented in Ichter et al. (2016), Loth et al. (2017)
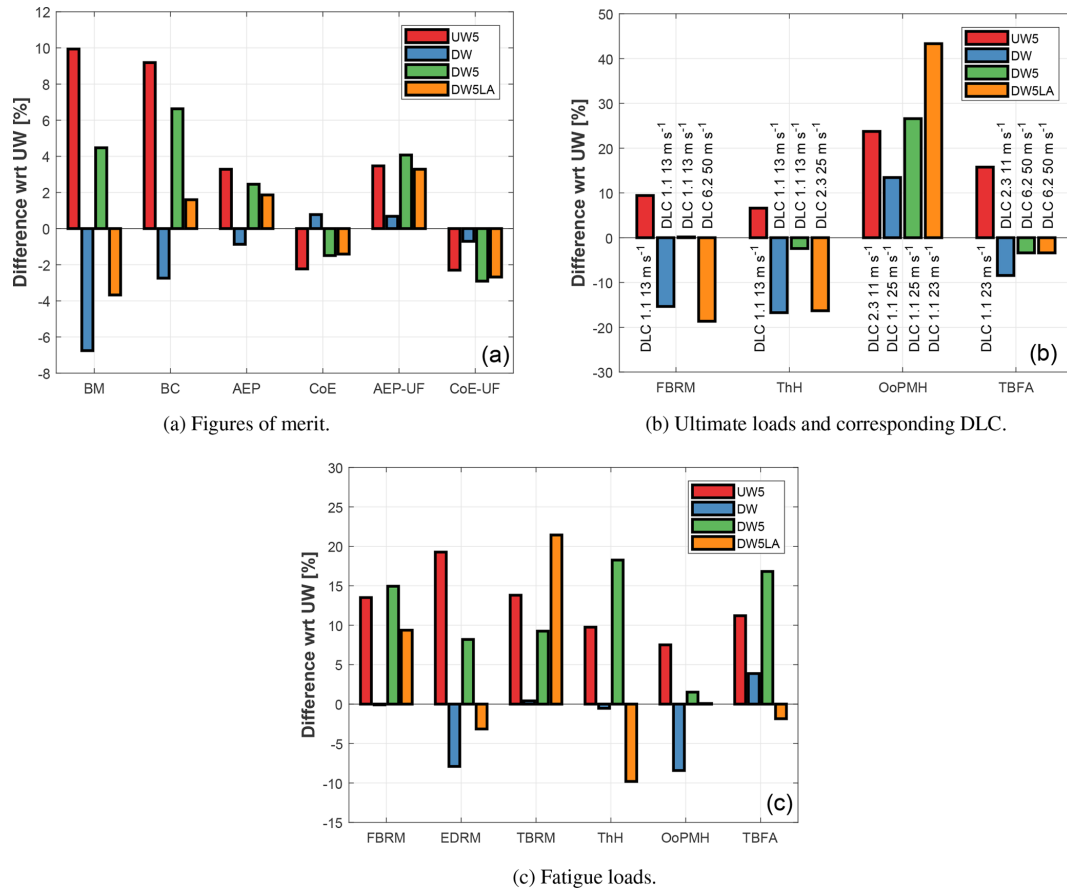
(a) Figures of merit.

(b) Ultimate loads and corresponding DLC.

(c) Fatigue loads.

Figure 4. Comparison in terms of main figures of merit (**a**), ultimate loads (**b**) and fatigue loads (**c**) for the four designs with respect to the baseline configuration UW. The CoE of DW5LA does not include the capital cost and power consumption of the active coning system in the calculations. Legend – BM: blade mass; BC: blade cost; UF: 5° of upflow; FBRM, EBRM and TBRM: flapwise, edgewise and torsional blade root moments, respectively; ThH and OoPMH: thrust and out-of-plane moment at the hub, respectively; TBFA: tower base fore–aft moment. In (**b**), the dominating DLCs of UW are the same of UW5.

and Noyes et al. (2018). This can be due to two main reasons. First, simplified analyses were conducted in Ichter et al. (2016), Loth et al. (2017) and Noyes et al. (2018), using steady-state conditions and no shutdown nor storm load cases, performing only a preliminary structural analysis. Secondly, the results presented in these studies adopt different design assumptions, including a two-bladed rotor with a constant γ (set to 17.5°). In the present work, the use of a constant γ was attempted, but proved to be ineffective for the current 10 MW case because of a dramatic reduction in AEP and of a limited load-alignment capability. In addition, a sufficiently high value of the coning rate appears to be necessary in highly turbulent wind conditions, such as the ones of the class 1A DTU 10 MW RWT considered here. These design choices differ from the ones assumed in the literature and, together with the arbitrary setting of the maximum blade root moment to 22 MNm, may affect the conclusions.

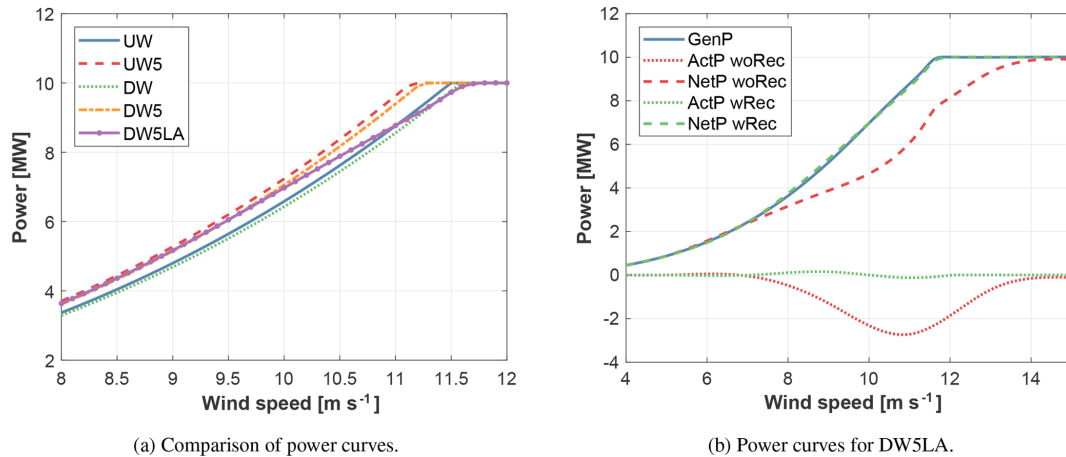Finally, a variable coning mechanism may raise major concerns in the presence of flap angle misalignments among the blades (for example, because of faults in one actuator or encoder), which could cause problematic rotor imbalances. Additionally, the case of partial or total power loss at the actuators should also be addressed and satisfactorily solved to ensure safety.

4 Conclusions and future work

This paper has presented a comparative study among five three-bladed upwind and downwind wind turbine configurations, with the aim of investigating the potential merit of downwind solutions and active load alignment in a 10 MW case. Based on the results reported herein, the following main conclusions can be drawn together with recommendations for future work.

4.1 Conclusions

First, downwind rotors help with limiting mass and cost of very large blades. Specifically, results indicate reductions of

(a) Comparison of power curves.

(b) Power curves for DW5LA.

Figure 5. Power generation for the five designs **(a)** and power consumption of the three coning actuators with and without recovery system (wRec and woRec, respectively). The efficiency of the recovery system is assumed to be equal to 80 %.

6 % in mass and 2 % in cost. It is speculated that further benefits could be obtained by optimized ad hoc shutdown strategies, which could help approach the slightly more promising conclusions exposed in Ning and Petch (2016). In addition, when the atmospheric flow is characterized by an upflow, such as in some complex terrain conditions, downwind machines generate a higher AEP than equivalent upwind designs because of a more favorable attitude of the rotor with respect to the incoming wind. In this study, a downwind rotor operating in a wind with an upflow of 5° generates 0.7 % more AEP than an equivalent upwind configuration. Any such increase, together with savings in blade cost, can lead to CoE reductions at approximately the same loading.

Secondly, generating an effective load alignment in highly turbulent wind conditions and storms appears to be a nontrivial task, even with an active solution. In addition, losses in AEP compared to traditional downwind designs are observed. These effects negatively impact the CoE. The power consumed by the three coning actuators is also nonnegligible, peaking for the configuration analyzed here at a staggering average of nearly 3 MW around rated wind speed. Without a power recovery system, this would dramatically impact the AEP. The extra investment for the three actuators, both in terms of capital and operational cost, is also expected to significantly impact the CoE. Finally, during storms, the usefulness of load alignment is very questionable, as the folding of a large rotor is unrealistic due to the resulting dramatic increase in hub and tower base moments.

Overall, conventional (nonconing) downwind designs are found to be more promising. These configurations could offer advantages either in conditions of marked atmospheric upflow or in the case of very large offshore machines, where blade mass needs to be limited. Having said this, it should also be remarked that the standard upwind solution appears to be very difficult to beat, even at these large sizes. Given the very significant body of knowledge and experience on

this configuration accumulated by industry so far, it remains to be seen whether the advantages of downwind solutions are worth the effort and risk that are undoubtedly necessary to bring them to full maturity.

4.2 Recommendation for future work

Additional investigations are necessary to address the assumptions and design decisions that may affect the conclusions of this work. For the comparison among UW, UW5, DW and DW5, an assessment of the effects of the four rotors on the design of the tower and of the nacelle components should be conducted. In addition, the blockage effect generated by the nacelle, which is not included in the present analysis, could possibly slightly improve the AEP and CoE of the downwind configurations. In this context, it would be useful to develop analytical corrections for BEM-based models to account for the presence of the nacelle in a downwind rotor. Furthermore, it is recommended to increase the number of turbulent seeds and possibly run the full list of DLCs as prescribed by international standards (IEC, 2005). Special attention should be given to the case of complex terrain installations. As suggested by Kress et al. (2015a) and the results reported in this paper, a downwind configuration may benefit in terms of AEP. However, an especially careful load assessment should be conducted as complex terrain conditions may also be characterized by increased unsteadiness in the wind, high shear and recirculation regions, which may result in higher loads on the turbine. Finally, a more rigorous holistic design optimization for upwind and downwind configurations should be conducted, including an optimization of the rotor diameter and an evaluation of the design for other wind turbine classes. In fact, the lower fidelity analyses conducted by Ning and Petch (2016) returned the greatest advantages of downwind configurations for class III machines.

Regarding the active coning solution, additional studies should assess the optimality of the design assumptions made so far, especially focusing on the amount of blade prebend, on the maximum flapwise blade root moment and on the coning rate. Finally, a more complete comparison with the existing literature should also consider the development of a teetering two-bladed downwind rotor, which was not studied here and might significantly change the conclusions.

References

Badyda, K. and Dylik, M.: Analysis of the impact of wind on electricity prices based on selected european countries, Energy Proced., 105, 55–61, https://doi.org/10.1016/j.egypro.2017.03.279, 2017.

Bak, C., Zahle, F., Bitsche, R., Kim, T., Yde, A., Henriksen, L. C., Andersen, P. B., Natarajan, A., and Hansen, M. H.: Description of the DTU 10 MW reference wind turbine, DTU Wind Energy Report-I-0092, July, 2013.

Bauchau, O. A.: Flexible Multibody Dynamics, Mechanics and Its Applications, Springer, ISBN:978-94-007-0335-3, 2011.

Bortolotti, P., Bottasso, C. L., and Croce, A.: Combined preliminary–detailed design of wind turbines, Wind Energ. Sci., 1, 71–88, https://doi.org/10.5194/wes-1-71-2016, 2016.

Bortolotti, P., Sartori, L., Croce, A., and Bottasso, C. L.: Integration of multiple passive load mitigation technologies by automated design optimization – The case study of a medium-size onshore wind turbine, Wind Energy, 22, 65–79, https://doi.org/10.1002/we.2270, 2018.

Bottasso, C. L., Croce, A., Savini, B., Sirchi, W., and Trainelli, L.: Aero-servo-elastic modeling and control of wind turbines using finite-element multibody procedures, Multibody Syst. Dyn., 16, 291–308, https://doi.org/10.1007/s11044-006-9027-1, 2006.

Bottasso, C. L., Croce, A., Nam, Y., and Riboldi, C. E. D.: Power curve tracking in the presence of a tip speed constraint, Renew. Energ., 40, 1–12, https://doi.org/10.1016/j.renene.2011.07.045, 2012.

Bottasso, C. L., Bortolotti, P., Croce, A., and Gualdoni, F.: Integrated aero-structural optimization of wind turbine rotors, Multibody Syst. Dyn., 38, 317–344, https://doi.org/10.1007/s11044-015-9488-1, 2016.

Frau, E., Kress, C., Chokani, N., and Abhari, R. S.: Comparison of performance and unsteady loads of multimegawatt downwind and upwind turbines, J. Sol. Energ.-T. ASME, 137, 041004-041004-8, https://doi.org/10.1115/1.4030314, 2015.

Giavotto, V., Borri, M., Mantegazza, P., and Ghiringhelli G.: Anisotropic beam theory and applications, Comput. Struct., 16, 403–413, https://doi.org/10.1016/0045-7949(83)90179-7, 1983.

Hansen, M. O. L.: Aerodynamics of Wind Turbines, 2nd Edn., Earthscan, London, ISBN: 978-1-84407-438-9, 2008.

Ichter, B., Steele, A., Loth, E., Moriarty, P., and Selig, M.: A morphing downwind-aligned rotor concept based on a 13-MW wind turbine, Wind Energy, 19, 625–637, https://doi.org/10.1002/we.1855, 2016.

INNWIND.EU, Deliverable 1.23, PI-based assessment of innovative concepts (methodology), INNWIND.EU technical report, Deliverable 1.23, available at: http://www.innwind.eu/Publications/Deliverable-reports (last access: June 2018), April 2014.

Johans, W. and Griffith, D. T.: Large Blade Manufacturing Cost Studies Using the Sandia Blade Manufacturing Cost Tool and Sandia 100-meter Blades, Sandia National Laboratories Technical Report, 2013.

Kress, C., Chokani, N., and Abhari, R. S.: Downwind wind turbine yaw stability and performance, Renew. Energ., 83, 1157–1165, https://doi.org/10.1016/j.renene.2015.05.040, 2015a.

Kress, C., Chokani, N., and Abhari, R. S.: Design Considerations of rotor cone angle for downwind wind turbines, J. Eng. Gas Turb. Power, 138, 052602-052602-10, https://doi.org/10.1115/1.4031604, 2015b.

Loth, E., Steele, A., Qin, A., Ichter, B., Selig, M. S., and Moriarty, P.: Downwind pre-aligned rotors for extreme-scale wind turbines, Wind Energy, 20, 1241–1259, https://doi.org/10.1002/we.2092, 2017.

Ning, A. and Petch, D.: Integrated design of downwind land-based wind turbines using analytic gradients, Wind Energy, 19, 2137–2152, https://doi.org/10.1002/we.1972, 2016.

Noyes, C., Qin, C., and Loth, E.: Pre-aligned downwind rotor for a 13.2 MW wind turbine, Renew. Energ., 116, 749–754, https://doi.org/10.1016/j.renene.2017.10.019, 2018.

Madsen, H. A., Johansen, J., Sørensen, N. N., Larsen, G. C., and Hansen, M. H.: Simulation of low frequency noise from a downwind wind turbine rotor, 45th AIAA Aerospace Sciences Meeting and Exhibit, Reno, Nevada, https://doi.org/10.2514/6.2007-623, 2007.

Manwell, J. F., McGowan, J. G., and Rogers, A. L.: Wind Energy Explained, Wiley, ISBN: 978-0-470-01500-1, 2009.

Peters, D. A. and He, C. J.: Finite state induced flow models-part II: three-dimensional rotor disk, J. Aircraft, 32, 323–333, https://doi.org/10.2514/3.46719, 1995.

Pitt, D. M. and Peters, D. A.: Theoretical prediction of dynamic inflow derivatives, Vertica, 5, 21–34, 1981.

Powles, S. R. J.: The effects of tower shadow on the dynamics of a HAWT, Wind Engineering, 7, 26–42, 1983.

Reiso, M.: The Tower Shadow Effect in Downwind Wind Turbines, PhD Thesis, Norwegian University of Science and Technology, 2013.

Sartori, L., Bortolotti, P., Croce, A., and Bottasso, C. L.: Integration of prebend optimization in a holistic wind turbine design tool, J. Phys. Conf. Ser., 753, https://doi.org/10.1088/1742-6596/753/6/062006, 2016.

Soltani, M. N., Knudsen, T., Svenstrup, M., Wisniewski, R., Brath, P., Ortega, R., and Johnson, K.: Estimation of rotor effective wind speed: a comparison, IEEE T. Contr. Syst. T., 21, 1155–1167, https://doi.org/10.1109/TCST.2013.2260751, 2013.

Wind Turbines Part 1: Design Requirements, Ed. 3, International Standard IEC 61400-1, available at: https://webstore.iec.ch/publication/5426&preview=1 (last access: 28 January 2019), 2005.